Applied Thermal Engineering 66 (2014) 335–345

Contents lists available at ScienceDirect

Applied Thermal Engineering

journal homepage: www.elsevier.com/locate/apthermeng

Development of a thermal oil operated waste heat exchanger within the off-gas of an electric arc furnace at steel mills

Christian Brandt [a,*], Nils Schüler [a], Matthias Gaderer [b], Jens M. Kuckelkorn [a]

[a] Bavarian Center for Applied Energy Research, Walther-Meißner-Str. 6, 85748 Garching, Germany
[b] Institute for Energy Systems, Technical University of Munich, Boltzmannstr. 15, 85748 Garching, Germany

HIGHLIGHTS

- EAF off-gas heat exchanger designs are restricted by high particle load.
- Heat exchanger configurations were designed based on analytical and numerical study.
- Particle cohesion between tubes and its compactness can be reduced.
- Heat exchanger design can be optimized adopting diagonal pitch-to-diameter ratio considering the permissible pressure drop.
- The numerical results for heat transfer and pressure drop deviated slightly from calculated analytical values.

GRAPHICAL ABSTRACT

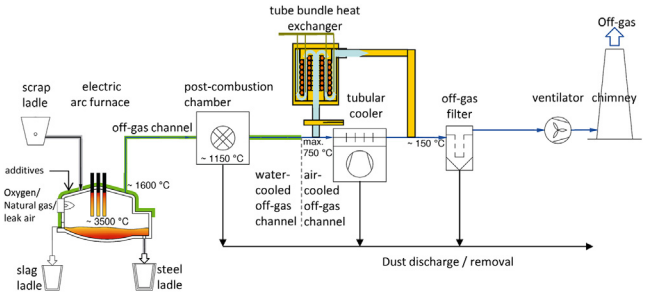

ARTICLE INFO

Article history:
Received 9 August 2013
Accepted 2 February 2014
Available online 14 February 2014

Keywords:
Electric arc furnace (EAF)
Discontinuous waste heat
Particle load
Tube bundle heat exchanger
Fouling
CFD simulation

ABSTRACT

A thermal oil operated tube bundle heat exchanger within the off-gas from an electric arc furnace (EAF) was developed for supplying heat to an electricity generating system by empirical methods. In this process both the unsteady heat flux and the dust load of the off-gas were considered.

A reference heat exchanger configuration was designed and optimized by empirical methods. Therefore in-situ experiments within the off-gas channel as well as parametric studies were undertaken. It was revealed that variations of geometric parameters have a positive impact on heat exchanger performance. The impact of the dust layer thickness on heat transfer and pressure drop was quantified.

A CFD model of a section of the reference heat exchanger configuration was generated using ANSYS CFX. Thus representative results for the complete heat exchanger were calculated and compared with the analytical results. The comparison of characteristic numerical results revealed a slight underestimation of heat exchange and pressure drop compared to analytical values.

1. Introduction

Considering the increasing global industrial energy demand [1] at shortage of resources and therefore rising energy costs, increasing the efficiency of industrial processes is of great importance. About 20% of the final energy demand in the manufacturing sector is from the global steel industry which amounted to approximately 23 EJ in 2005 [2]. Thirty-two percent of the steel is

Abbreviations: AAS, atomic absorption spectroscopy; CFD, computational fluid dynamics; EAF, electric arc furnace; EDX, energy-dispersive X-ray spectroscopy; SEM, scanning electron microscope; ORC, Organic Rankine Cycle.

* Corresponding author. Tel.: +49 89 329442 82; fax: +49 89 329442 12.
E-mail addresses: christian.brandt@zae-bayern.de, brandt@muc.zae-bayern.de (C. Brandt).

http://dx.doi.org/10.1016/j.applthermaleng.2014.02.003
1359-4311/

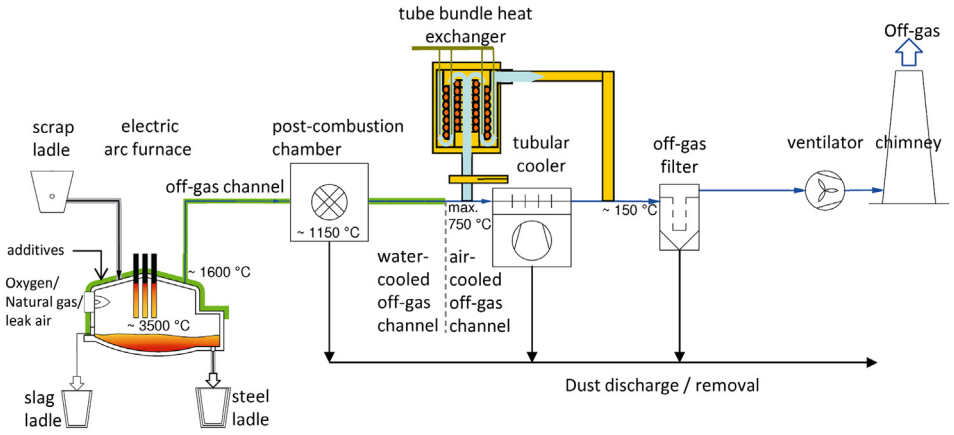

Fig. 1. Measurement and heat exchanger location within the direct evacuation of the EAF. The heat exchanger is located after the water-cooling system of the off-gas channel, in front of the tubular cooler.

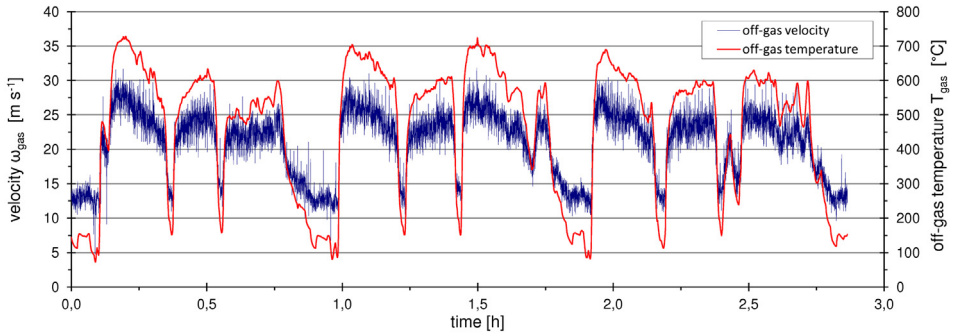

Fig. 2. Typical off-gas temperature and velocity during three melting cycles.

produced using electric arc furnaces (EAF) [2], where scrap metal is melted using an electric current [1].

As the steel production is increasing, the total power demand is growing [3,4]. Hence enhancing energy efficiency of steel production processes contributes to the reduction of primary energy demand and thereby the achievements of climate protection targets. At steel plants up to 35% of the required energy exhausts via the off-gas channel system [5], revealing a great potential to increase the total energy efficiency.

The overall objective of this project was the development of a concept to use this waste heat for power generation, using an Organic Rankine Cycle (ORC), and thus to reduce CO_2 emissions [28]. Current waste heat recovery technologies were employed for power generation using low temperature waste heat. For the EAF process, characteristic off-gas parameters like temperature and particle load were not available. Hence the challenge was to measure these values and design a heat exchanger to operate an ORC. The content of this publication focuses on the design of a feasible heat exchanger concept under fouling conditions in the EAF off-gas environment.

2. Basic examinations

2.1. Off-gas measurements

The off-gas measurements comprised the in-situ measurements of off-gas temperature, static and dynamic pressure, particulate matter as well as the offline measurements of thermal conductivity, the analysis of EAF dust composition, slagging and melting characteristics and corrosion potential.

Due to the batch operation of the EAF, the discontinuous availability of waste heat had to be analyzed. The measurements were conducted within the off-gas system in front of the tubular cooler with state-of-the-art measurement equipment (Fig. 1).

Off-gas temperature T_{gas}, static pressure p_{stat}, and dynamic pressure p_{dyn}, were measured over several melting cycles to record reliable off-gas data and thus to determine off-gas velocity, flow rate and enthalpy. The apertures of the Pitot tubes used are object to fouling. Thus an automated cleaning system for the measuring apertures was developed which was operated with compressed air. Measured characteristic off-gas temperatures and velocities are shown in Fig. 2 for three melting cycles.

Each melting process lasts approximately 50 min. The replacement of the liquid steel tank by a refilled scrap ladle lasts five to 10 min. The total process until tapping of the liquid steel lasts between 55 and 60 min. At this steel mill, off-gas temperatures reached maximum values between 750 °C and 796 °C at tapping, between 120 °C and 160 °C during charging and short-term interruptions, and decrease to about 60 °C for longer plant operation breaks. The average off-gas temperature is approximately 550 °C. Table 1 shows the characteristic off-gas parameters of the investigated EAF.

Table 1
Off-gas parameters in front of the tubular cooler.

		Average	Minimum	Maximum
Temperature off-gas	T_{gas} [°C]	550	64	796
Static pressure	$p_{stat,gas}$ [Pa]	96359.8	96179.5	96715.0
Dynamic pressure [Pa]	$p_{dyn,gas}$ [Pa]	−200.3	−481.2	−101.6
Density	ρ_{gas} [kg m^{-3}]	0.5	0.3	1.0
Velocity	w_{gas} [m s^{-1}]	24.7	12.2	41.1
Mass flow	$\dot{m}_{gas}$ [kg s^{-1}]	19.8	12.8	30.9

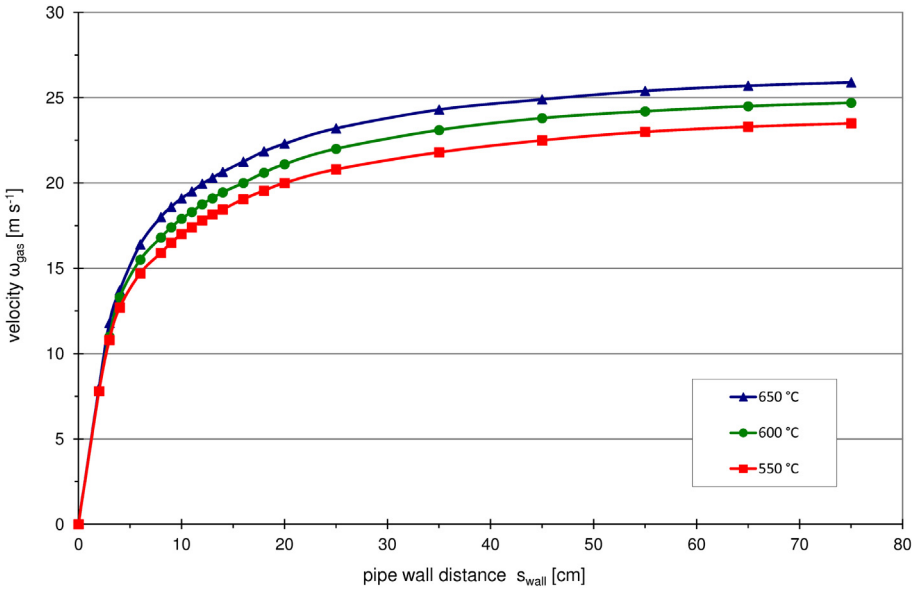

Fig. 3. Interpolated velocity profile over the cylindrical off-gas channel at 550 °C, 600 °C and 650 °C: The values over several minutes during the melting process are time averaged.

The calculated Reynolds number *Re*, to evaluate the flow character is more than 100 times the critical value of *Re* (≈2300). Thus the flow is turbulent.

$$Re = \frac{w_f D}{\nu} \tag{1}$$

A profile of the off-gas velocity distribution from the channel wall towards the core off-gas stream was measured and evaluated to derive the average velocity w_f and mass flow. Fig. 3 shows a similar off-gas velocity distribution over the radius of the cylindrical off-gas channel ($D/2 = 750$ mm) for different temperatures. Only near the channel wall is the influence of channel friction visible.

The off-gas composition varies with the scrap composition as well as with the operating point of steelmaking process (e.g. at decarburization). Further it depends on the position of measurement within the off-gas channel system. Reliable off-gas composition data were recorded by Kirschen [5] and Voj [8] for various EAF dimensions. Appropriate data were used for the determination of the off-gas density and heat conductivity.

2.2. Characterization of EAF dust

The knowledge of the chemical composition of dust emitted by the EAF is important for the identification of the driving corrosion mechanisms and thus for the material selection for the heat exchanger. The chemical composition of EAF dust sampled in front of the tubular cooler (Fig. 1) was analyzed by different quantitative and semi-quantitative methods (EDX/SEM, AAS and X-ray fluorescence analysis). Fig. 4 shows the identified chemical composition of EAF dust which was in the same range as those values from other comparable publications [9–11]. Due to scrap composition, metals (Fe, Zn) as well as alkaline and alkaline earth elements (e.g. K, Ca, Mg) occur. The chlorine fraction is 5 mol% (wet chemical pulping) what leads to chlorine corrosion.

A 6 month online corrosion measurement with a probe system from the company Corrmoran GmbH revealed that corrosion is the driving force for material loss and not only abrasion due to high particle velocity. The corrosion was electrochemically measured with a proofed probe system [12]. Current corrosion rates were quantitatively determined for the materials S235JR + AR (St37-2) and 16Mo3 proving the higher physical resistance of higher alloyed

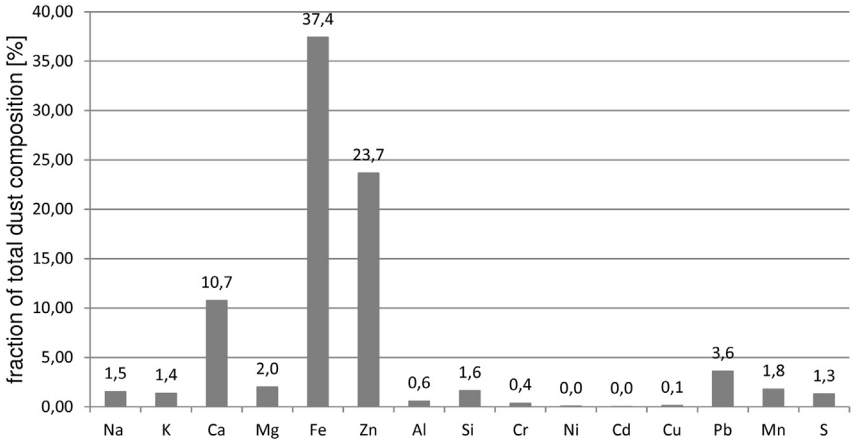

Fig. 4. Chemical mass-composition of EAF dust: The dominating influence of Zn and Fe is related to the scrap composition.

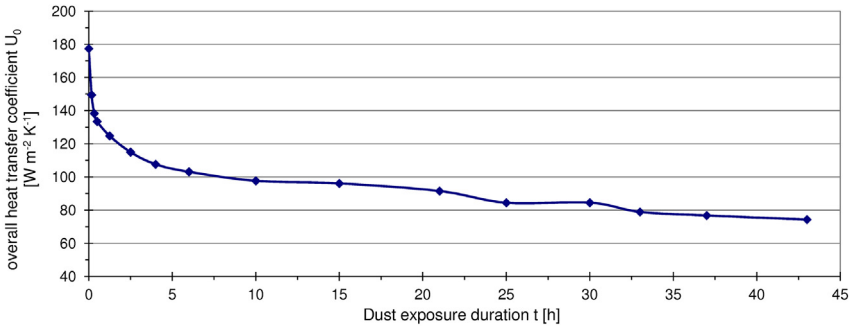

Fig. 5. Development of the measured heat transfer coefficient as a function of dust deposit time: significant deterioration of the heat transfer coefficient within first hour, a slower decrease after 10 h.

steels. Even higher corrosion resistance was revealed for the stainless steel 1.4571 (X6CrNiMoTi17-12-2). Thus its material parameters were used for the calculations and CFD simulations of the heat exchanger designs (Section 3).

Also the fouling factor R_f, whose value can be interpreted as a thermal resistance, as well as the thermal conductivity are necessary for the heat transfer calculations and simulations (Section 3). There were no reliable values for the thermal conductivity and the fouling factor of EAF-dust in literature or from steel mills to date. Therefore extensive measurements and simulations were conducted. The fouling factor was determined to be $R_f = 0.0041\ m^2\ K\ W^{-1}$ for an average layer thickness of 1.5 mm. The value of particle load in wet off-gas was calculated as 9.5 gm^{-3}.

2.3. Tube sample tests

As the dust layer thickness limits the heat transfer and varies considerably with tube diameter and tube exposure, comprehensive tube sample tests were conducted to identify suitable tube geometries and arrangements. The objective was to minimize dust adhesion and thus to reduce the impact of the dust layer on heat transfer and the effort to clean the heat exchanger tubes (Section 4). Thus various tube configurations (in-line/staggered), tube profiles (electropolished/smooth/finned), tube bundles with different pitch-to-diameter ratios and inflow directions (stream- or crosswise to flowing direction) were tested without cooling or measurement instrumentation within the off-gas channel system in front of the tubular cooler.

The tube sample tests showed that tubes oriented parallel to the off-gas stream are covered by less dust deposits than those crosswise oriented ones to the flowing direction. For crosswise oriented tubes it could be confirmed that dust layer thickness decreases with increasing tube diameter. Tube bundle tests with up to 11 tubes revealed that particle cohesion between the tubes is less compacted if the tubes are oriented crosswise. The turbulence in crosswise bundles is increased in comparison to streamwise ones and is further increased for a staggered tube arrangement instead of an in-line arrangement. Increased turbulence enhances the heat transfer in crossing tube bundles. The pitch-to-diameter ratio also plays a major role in particle deposition and particle cohesion [13]. It was experimentally found that the diagonal pitch-to-diameter ratio must be at least $c = 2.0$ to avoid an entirely fouling of the tube bundle.

2.4. Heat transfer measurements

A dummy heat exchanger with a measuring sensor system was developed and operated within the off-gas channel system to identify and quantify the influence of high particle load and the impact of non-operation periods on heat transfer. The tube wall temperature of the heat exchanger at the end of the measuring section was maintained at 350 °C by the controlled flow of compressed air. The measurements were operated with and without dust layers. After 0.25 h, 1 h, 20 h and 40 h the dummy heat exchanger was gathered from the off-gas channel system and hence the dust layer was observed and its thickness measured. After observation the dust layer was removed from the tube surface to gain sufficient reference measurement data for the cleaned tube surface state.

At the beginning of measurement, the measured thermal heat flow showed similar values as those calculated according to VDI heat atlas [15]. Until a measurement time of 30 min it decreased up to 25%, compared to an unfouled tube surface. After 30–50 min the measured heat flow further decreased with increasing dust layer thickness. After 10 h, the measured heat transfer coefficient decreased to 55% of the initial value without dust deposit and further deteriorated to 45% after 40 h (Fig. 5). The rate of deterioration of the measured heat transfer coefficient clearly slowed down after 10 h as the rate of growth of the dust layer slowed down due to the off-gas flow, which is responsible for removal of the upper dust layer. Thus the heat transfer is not completely suppressed by the dust layer but reduced to a minimum value.

3. Heat exchanger design

Based on the comprehensive examinations in terms of EAF dust mass, dust exposure and heat transfer, various waste heat exchanger configurations were determined and evaluated. The overall objectives for the heat exchanger design were:

- a high thermal oil outlet temperature
- a high heat transfer rate
- minimum pressure drop (off-gas/thermal oil)
- affordable but preferably corrosion and heat resistant material
- feasible preparation and installation of the heat exchanger on site
- appropriate safety and control engineering instrumentation

3.1. Analytical approach

3.1.1. General specifications

One general specification of the waste heat recovery concept was the cooling of the off-gas to at least 150 °C as required for the bag filters of the steel plant (Fig. 1). The existing tubular cooler should be replaced by the waste heat exchanger to save electrical auxiliary power. Further, the off-gas pressure drop was not allowed to exceed 1000 Pa since the blower after the bag filter is not able to

Table 2
Specified flow parameters of off-gas and thermal oil.

	Location		Off-gas	Thermal oil
Temperature	Inlet	T_{in} [°C]	160–450	100
	Outlet	T_{out} [°C]	150	≤350
Pressure	Inlet	p_{in} [bar]	0.96	>1.5
	Outlet	p_{out} [bar]	≥0.95	≥1.5

compensate a higher pressure drop. The minimum outlet pressure results from the subtraction of the maximum permissible pressure drop from the measured static pressure at the inlet of approximately 0.96 bar (Table 1). The heat recovery system must not disturb the steel production process. In terms of the waste heat exchanger, appropriate cleaning, revision and substitution facilities for the tube bundles, as well as safety and control engineering, i.e. separation possibilities if set up within a by-pass, must be provided.

For the thermal oil circuit, the properties of the chosen thermal oil determined the maximum inner wall temperature. Therminol® 66 is a suitable silicone oil with a vapor pressure of 1.5 bar and a film temperature of 359 °C. Thus a maximum permissible inner tube wall temperature of 350 °C guarantees the thermal stability of the thermal oil. The heat exchanger was designed to provide a turbulent flow of the thermal oil throughout the tubes. Thereby both a more uniform temperature distribution within the thermal oil and a maximum inner wall heat transfer coefficient is attained. These requirements are summarized in Table 2.

Table 3 lists the geometric parameters which were experimentally determined.

Table 4 lists the material parameters derived from the off-gas and heat transfer measurements (Section 2.4).

3.1.2. Empirical correlations

The experimentally determined parameters were used together with empirical correlations according to VDI heat atlas [15] and [18–27] to design the heat exchanger.

The overall heat transfer coefficient in relation to the outer surface U_o is a characteristic parameter for the heat exchanger. For a tube it is calculated by:

$$U_o = \frac{1}{\frac{1}{\alpha_{gas}} + d_o \pi l_{tube} R_f + \frac{d_o}{2\lambda_{steel}} \ln\left(\frac{d_i}{d_o}\right) + \frac{d_o}{\alpha_{oil} d_i}} \tag{2}$$

with the inner and outer tube diameter d_i and d_o, respectively, the length of a tube l_{tube}, the fouling factor R_f and the heat conductivity of steel λ_{steel}. The heat transfer coefficient on the off-gas side of tubes in a tube bundle α_{gas} is calculated using the Nusselt number Nu_{bundle}, which is the dimensionless heat transfer coefficient:

$$\alpha_{gas} = \frac{Nu_{bundle} \lambda_{gas}}{L} \tag{3}$$

The stream length of a tube is the characteristic length $L = 0.5\pi d_o$.

For an entire tube bundle of more than 10 consecutive rows the Nusselt number is computed from:

$$Nu_{bundle} = f_A Nu_{row} \tag{4}$$

Table 3
Specified geometric parameters of the heat exchanger tubes and the off-gas channel.

Outer oil tube diameter	d_o [mm]	48.3
Inner oil tube diameter	d_i [mm]	41.8
Inner off-gas channel diameter	D [mm]	1500

Table 4
Specified material parameters of the dust and the heat exchanger tubes.

		Dust	Steel[a]
Heat conductivity	λ [W m^{-1} K^{-1}]	0.35	15
Fouling factor (d_a = 48.3 mm)	R_f [m^2 K W^{-1}]	0.0041	–
Dust layer thickness (d_a = 48.3 mm)	s_d [mm]	1.5	

[a] For stainless steel 1.4571 (X6CrNiMoTi17-12-2).

with a tube arrangement factor f_A. For a staggered arrangement it is only affected by the streamwise pitch-to-diameter ratio b:

$$f_{A,stag} = 1 + \frac{2}{3b} \tag{5}$$

Assuming a quadratic tube arrangement the correlations between the crosswise, streamwise and diagonal pitch-to-diameter ratios a, b and c are:

$$\begin{aligned} c &= \sqrt{(0,5a)^2 + b^2} \\ a &= 2b \end{aligned} \tag{6}$$

The Nusselt number for one row is calculated from:

$$Nu_{row} = 0.3 + \sqrt{Nu_l^2 + Nu_t^2} \tag{7}$$

with a laminar l and a turbulent t component:

$$\begin{aligned} Nu_l &= 0.664 \sqrt{Re_\psi} \sqrt[3]{Pr} \\ Nu_t &= \frac{0.037\, Re_\psi^{0.8} Pr}{1 + 2.443\, Re_\psi^{-0.1} (Pr^{2/3} - 1)} \end{aligned} \tag{8}$$

The Prandtl number Pr accounts for the fluid properties and is calculated using the values for an arithmetic average of the inlet and outlet fluid temperatures.

These equations are valid for

$$\begin{aligned} 10 &< Re_\psi < 10^6 \\ 0.6 &< Pr < 10^3 \end{aligned} \tag{9}$$

with a Reynolds number defined as:

$$Re_\psi = \frac{w_f L}{\psi \nu} \tag{10}$$

w_f denotes the average velocity obtained in the free cross section in front of the tube bundle. The void fraction ψ is calculated using the crosswise pitch-to-diameter ratio a.

$$\psi = 1 - \frac{\pi}{4a} \quad \text{for } b \geq 1 \tag{11}$$

The pressure drop across a tube bundle for which gravitational effects can be neglected is:

$$\Delta p_{tot} = \Delta p_f + \Delta p_a \tag{12}$$

The term Δp_f accounts for friction:

$$\Delta p_f = \xi n_o \frac{\rho w_n^2}{2} \tag{13}$$

The number of main obstacles in flow direction n_o equals the number of rows in this direction if $b \geq 0.5\sqrt{2a+1}$ and w_n is the average velocity in the narrowest section within the tube bundle.

This velocity is also used for another definition of the Reynolds number:

$$Re = \frac{w_n d_o}{\nu} \tag{14}$$

This definition is valid for all of the following pressure-related equations for tube bundles.

The friction factor for a staggered tube arrangement is:

$$\xi = \xi_l f_{zn,l} + \left(\xi_t f_{z,t} + f_{n,t}\right) \left(1 - \exp\left(-\frac{Re+200}{1000}\right)\right) \tag{15}$$

containing correction factors for temperature dependence f_z and number of rows f_n or a combination of both f_{zn}

$$\begin{aligned} \xi_l &= \frac{f_{A,l,\mathrm{stag}}}{Re} \\ f_{A,l,\mathrm{stag}} &= \frac{280\pi\left(\left(b^{0.5}-0.6\right)^2+0.75\right)}{(4ab-\pi)a^{1.6}} \\ f_{zn,l} &= f_{z,l} \quad \text{for } n_{\mathrm{rows}} \geq 10 \\ f_{z,l} &= \left(\frac{\eta_W}{\eta}\right)^{\left(0.57((4ab/\pi-1)Re)^{-0.25}\right)} \end{aligned} \tag{16}$$

and a turbulent component

$$\begin{aligned} \xi_t &= \frac{f_{A,t,\mathrm{stag}}}{Re^{0.25}} \\ f_{A,t,\mathrm{stag}} &= 2.5 + \left(\frac{1.2}{(a-0.85)^{1.08}}\right) + 0.4\left(\frac{b}{a}-1\right)^3 - 0.01\left(\frac{a}{b}-1\right)^3 \\ f_{n,t} &= 0 \quad \text{for } n_{\mathrm{rows}} \geq 10 \\ f_{z,t} &= \left(\frac{\eta_W}{\eta}\right)^{0.14} \end{aligned} \tag{17}$$

Index w denotes all fluid properties which have to be calculated for an average wall temperature T_w.

If a compressible fluid undergoes significant changes in temperature, a pressure drop due to acceleration Δp_a has to be considered and is calculated using the free stream velocities and fluid densities in front of and behind the tube bundle. For a constant cross section the pressure drop due to acceleration is:

$$\Delta p_a = \left(\rho w_f^2\right)_{\mathrm{out}} - \left(\rho w_f^2\right)_{\mathrm{in}} \tag{18}$$

3.1.3. Sensitivity analysis of variable input parameters

In order to design and optimize the heat exchanger, the influence of the diagonal pitch-to-diameter ratio on heat transfer and pressure drop was examined. Given a fixed number of crosswise tubes per row and a constant tube length, an increasing diagonal pitch-to-diameter ratio c leads to an increasing cross section of the heat exchanger.

Fig. 6 shows the effect of an increasing cross section on the pressure drop and the overall heat transfer coefficient related to the outer tube surface U_o: For a constant volume flow rate, an increasing cross section decreases the velocity and Reynolds number, respectively, which results in both decreased pressure drop and heat transfer. In order to enhance heat transfer the cross section should be as small as acceptable regarding the permissible pressure drop.

In order to save costs, tubes with standard length of $l_{\mathrm{tube}} = 3$ m were chosen. For a fixed tube length and an increasing diagonal pitch-to-diameter ratio the cross section can be kept small by reducing the number of tubes per row. In Fig. 7 this number is reduced as soon as it does not lead to an impermissible pressure drop. Consequently the heat exchanger design was slightly

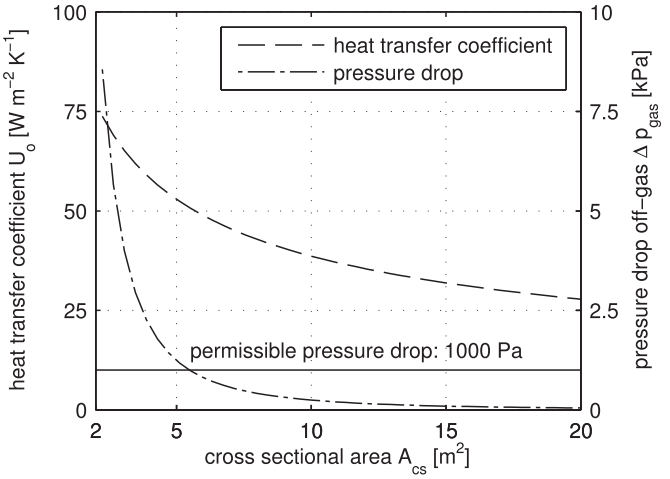

Fig. 6. Influence of the cross section of the heat exchanger on heat transfer and pressure drop.

enhanced by chosing a diagonal pitch-to-diameter ratio of 2.05 instead 2.0, which was the experimentally determined least permissible ratio due to fouling. Thus the cross sectional area of the heat exchanger was reduced despite of an increased distance between the tubes.

Based on the general specifications and conducted sensitivity analyses, an optimized heat exchanger configuration was identified.

3.1.4. Calculated heat exchanger configuration

For the heat exchanger design the highly unsteady flow conditions of the off-gas were considered. The off-gas mass flow rate is nearly constant and its density is temperature dependent. Therefore the highest velocity and permissible pressure drop in the channel is reached for the highest measured off-gas temperature of approximately 750 °C. This must be considered when designing the geometry of the heat exchanger. The mean temperature, however, is approximately 550 °C (Section 2.1). This design point was chosen for the following calculations resulting in an oversized heat exchanger for most of the occurring operating points, thus guaranteeing the intended heat transfer. The oversizing for higher temperatures results in an undercooling of the off-gas below the desired temperature of 150 °C which is acceptable. The operating points at lower temperatures are the more critical ones as the heat

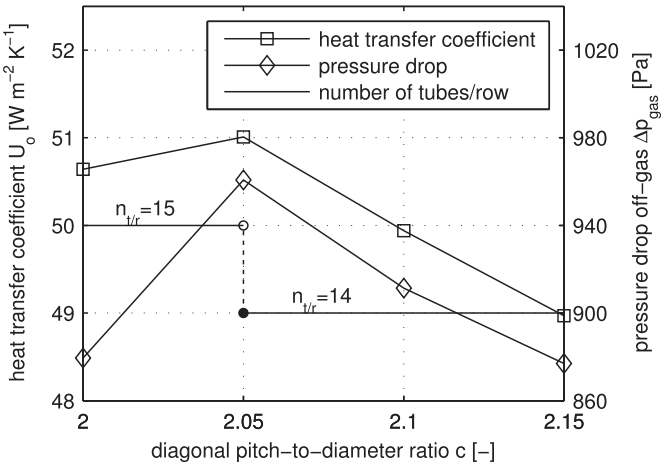

Fig. 7. Influence of the diagonal pitch-to-diameter ratio on heat transfer, pressure drop and related number of tubes per row ($T_{\mathrm{in,gas}} = 750$ °C).

Table 5
Geometric parameters of the optimized heat exchanger configuration.

Diagonal pitch-to-diameter ratio	c	2.05	Length of tubes	l_{tube} [m]	3
Total number of tubes	n_{tubes}	2408	Width of entire bundle	W_{bundle} [m]	2
Number of tubes per row	$n_{t/r}$	14	Length of entire bundle	L_{bundle} [m]	12
Number of rows	n_{rows}	172	Cross sectional area	A_{cs} [m^2]	6
Passings of thermal oil	n_{oil}	180	Heat exchanger area	A_{hx} [m^2]	1096

Table 6
Flow parameters of the optimized heat exchanger configuration for different operation points (i.e. off-gas temperatures).

Off-gas					
Inlet temperature	$T_{in,gas}$ [°C]	450	550	650	750
Outlet temperature	$T_{out,gas}$ [°C]	159.8	150.1	144.8	141.6
Pressure drop	Δp_{gas} [Pa]	732.7	807.2	883.9	960.7
Thermal oil					
Outlet temperature	$T_{out,oil}$ [°C]	333.1	336	335.4	333.2
Outlet pressure	$p_{out,oil}$ [bar]	4.22	3.57	2.72	1.61
Mass flow	$\dot{m}_{oil}$ [kg s^{-1}]	8.336	11.52	14.8	18.23
Average Reynolds number	$\overline{Re}_{oil}$ [−]	25523	34598	43918	53488
Heat transfer					
Heat transfer coefficient off-gas	α_{gas} [W m^{-2} K^{-1}]	62.53	65.26	67.87	70.37
Heat transfer coefficient thermal oil	α_{oil} [W m^{-2} K^{-1}]	698.4	913.7	1127	1342
Overall heat transfer coefficient	U_o [W m^{-2} K^{-1}]	44.98	47.29	49.25	51.01
Intended heat flux	$\dot{q}_{int}$ [kW]	4610	6215	7856	9532
Transferable heat flux	$\dot{q}_{able}$ [kW]	3965	6210	8290	10321

exchanger is not able to cool down the off-gas to the desired outlet temperature. This has to be considered especially if the heat exchanger is not placed within a by-pass. The geometric and flow parameters characterizing the most favorable heat exchanger configuration are summarized in Tables 5and 6.

3.2. Simulations

This heat exchanger configuration was validated using a steady-state CFD simulation of the tube bundle covered by a dust deposition layer of 1.5 mm average thickness. The simulations were performed with ANSYS CFX 14.0. The appropriate tools of ANSYS Workbench were used for all of the required meshing, pre- and postprocessing tasks.

3.2.1. Model

Modeling the entire heat exchanger exceeded the available computational resources. Thus representative results were gained by modeling three different sections of the heat exchanger in the flow direction of the off-gas [16]. From these results, average values for the entire heat exchanger were estimated. The different sections were modeled by applying different boundary conditions to the same geometric model.

In order to model fully developed boundary layers around the tubes, 10 consecutive rows in flow direction were modeled. In addition the inlets and outlets of the off-gas were placed at sufficient distance from the tube bundle to prevent any unintended numerical effect. This distance was chosen as 10 times the outer tube diameter d_o.

The model size could be further reduced by using all available symmetry planes. Thus only one central streamwise channel with half a tube cross section was modeled. The tubes had to be

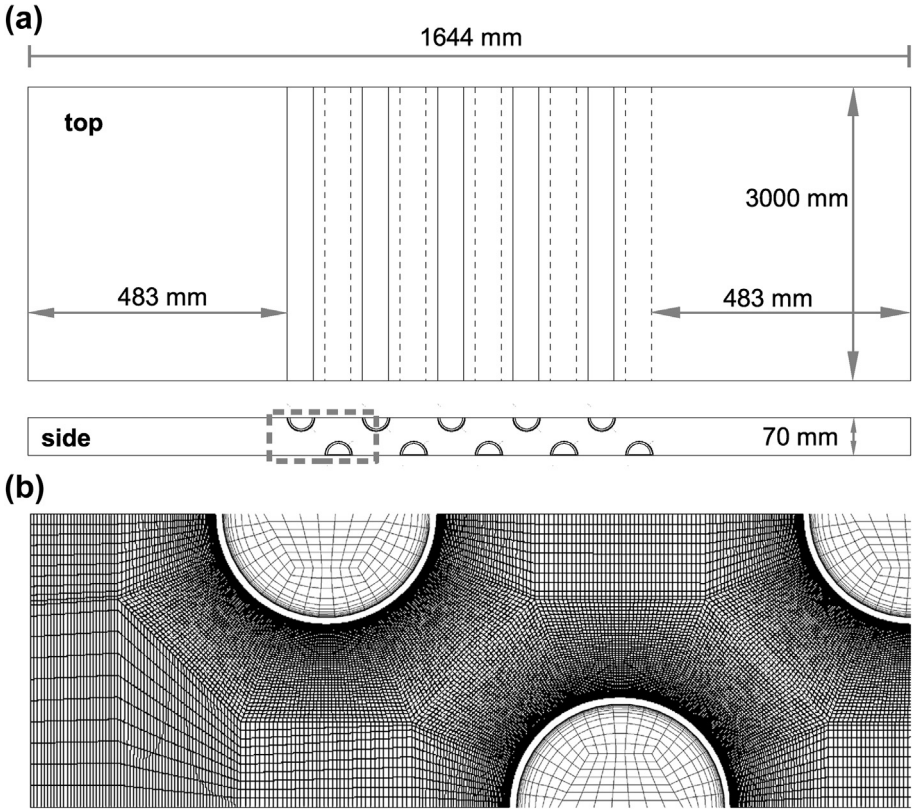

Fig. 8. Simulation model geometry and mesh. (a) Dimensions of the model in top and side view (location of mesh detail indicated). (b) Detail of mesh in side view.

integrated with their full length of 3 m because of the cross flow design of the heat exchanger. These requirements resulted in the model depicted in Fig. 8(a).

3.2.2. Domain definitions

Within this model three different domains were defined. The off-gas was modeled as an ideal gas. This assumption was justified by previous experiments. The properties of Therminol® 66 were used for modeling the thermal oil. The tubes were assumed to be made from stainless steel as specified in Table 4.

Instead of defining a domain for the dust deposition layers around the tubes, their thermal resistance was modeled by specifying the experimentally determined fouling factor at the interfaces between tubes and off-gas (Table 4). This resulted in gaps in the model around each tube. Hence the required number of cells and thereby computational costs were further reduced. For simplicity the dust layer in the model was supposed to have a constant thickness of 1.5 mm around the tubes.

3.2.3. Boundary conditions

No slip was specified at the boundary faces of each gap towards the off-gas domain, the inner tube surfaces towards the thermal oil domain and the side walls of the off-gas domain. Symmetry conditions were applied for all domains at top and bottom of the model.

The thermal oil flows through consecutive tubes against the off-gas flowing direction. Instead of modeling manifolds between the tubes, the inlet and outlet conditions of the single tubes were set appropriately. Each inlet temperature was set to the average temperature determined at the previous outlet upstream (Fig. 9) The inlet temperature of the first tube was set to the values specified in Table 7. To account for correct flow patterns at the inlets and outlets of the tubes, velocity and pressure fields were determined through previous simulations of oil flow in tubes with manifolds and were applied to the inlets and outlets, respectively, of all tubes. Depending on the modeled section of the heat exchanger, the boundary conditions at the inlet and outlet of the off-gas domain were set according to Table 7.

3.2.4. Solver parameters

CFX's Shear Stress Transport model with automatic wall treatment was employed to account for turbulence [17]. All solutions were obtained with normalized residuals less than 10^{-5}.

3.2.5. Mesh

All domains were regularly meshed with hexahedrons. A detail view can be seen in Fig. 8(b). In order to resolve the boundary layers, all meshes were refined towards the tube walls so that the dimensionless wall distances y^+ of adjacent cells were approximately one. This distance is a characteristic number used to evaluate the mesh near the tube wall. Separate mesh studies for the off-gas and thermal oil domains were performed to identify mesh resolutions which satisfy both discretization error and computational costs. Because of model size and required resolution the optimized meshes contained still almost 31 million cells in total.

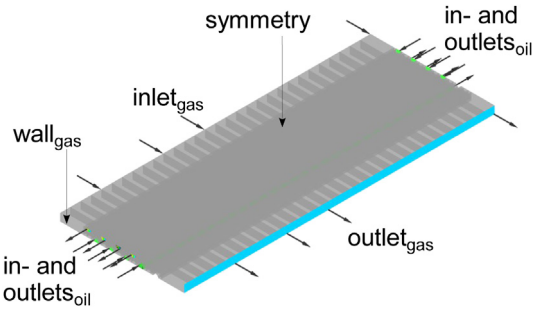

Fig. 9. Boundary conditions of the simulation model.

Table 7
Boundary conditions for each modeled section of heat exchanger.

Section		First	Middle	Last
Rows (total: 172)	n_{rows}	1–10	83–92	163–172
Off-gas				
Inlet velocity	$w_{in,gas}$ [m s^{-1}]	5.94	4.12	3.08
Inlet temperature	$T_{in,gas}$[°C]	550.0	297.3	161.4
Relative[a] pressure outlet	$p_{rel,gas}$ [Pa]	−46.93	−431.8	−807.2
Thermal oil				
Inlet temperature first tube	$T_{in,gas,1}$ [°C]	316.7	176.9	101.2
Inlet velocity all tubes	$w_{in,oil}$ [m s^{-1}]	Velocity fields (average: 0.8)		
Outlet pressure all tubes	$p_{out,oil}$ [bar]	Pressure fields		
Reference pressure all tubes	$p_{ref,oil}$ [bar]	3.568	4.284	5.000

[a] Reference pressure: 0.96 bar.

3.2.6. Results

Different parameters were employed to compare numerical and analytical results:

- convection heat transfer coefficients for off-gas α_{gas} and thermal oil α_{oil}
- overall heat transfer coefficient in relation to the outer tube surface U_o
- heat flux $\dot{q}$
- pressure drop of off-gas Δp_{gas}

The numerical values of these parameters were calculated at the eighth tube of the model. Fully developed flow can be assumed for this tube because of the distance towards inlet and outlet of the modeled tube bundle. Thus influences of the geometric model on the numerical results were decreased. In contrast the heat transfer at downstream tubes does not affect the boundary layers at the eighth tube. Therefore no thermal oil flow through the last two tubes relatively to the direction of the off-gas flow was simulated, further reducing the required number of cells.

The simulated velocity and temperature distributions at the beginning of the heat exchanger (Fig. 10) represent the expected flow conditions plausibly with high off-gas velocities between the tubes and reduced velocities in the wakes of each tube. This results

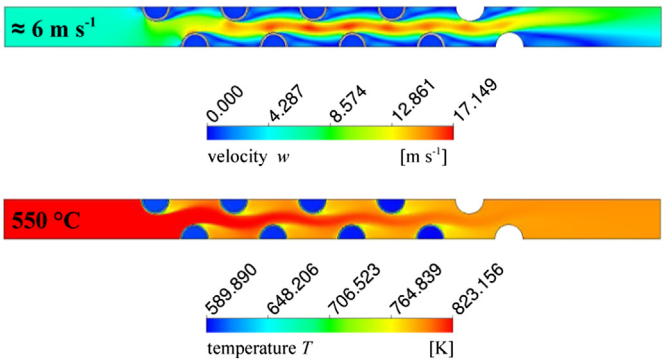

Fig. 10. Numerically calculated velocity and temperature distributions at the beginning of the heat exchanger: Highest off-gas velocities and thereby high heat transfer rates occur at the sides of the tubes, where they lead to lower temperatures. The turbulence in the wakes of the tubes leads to a more uniform temperature distribution in these areas.

Table 8
Numerical and analytical results for the heat exchanger and deviation of numerical results from analytical results using a cubic spline interpolation for the numerical results of the three different sections.

	α_{gas} [W m^{-2} K^{-1}]	α_{oil} [W m^{-2} K^{-1}]	U_o [W m^{-2} K^{-1}]	$\dot{q}$ [W m^{-2}]	Δp_{gas} [Pa]
Numerical results					
Beginning of heat exchanger	55.3	1401.8	41.7	8.73	5.67
Middle of heat exchanger	54.3	802.7	40.1	4.35	4.07
End of heat exchanger	52.6	401.9	37.0	2.02	3.10
Average	54.1	836.1	39.9	4.70	4.18
Analytical results (reference)	65.3	913.7	47.3	5.67	4.69
Deviation [%]	−17.2	−8.5	−15.6	−17.1	−10.9

in high heat transfer rates at the sides of the tubes depicted by high temperature gradients. The temperature distribution in the wakes of the tubes is more uniform due to the local higher turbulence in this regions.

For each parameter the numerical values of the three sections were averaged using a cubic spline interpolation. The averaged values were compared with the analytical ones by determining the deviation of the average numerical value from the analytical result for the whole heat exchanger (Table 8, Fig. 11).

With around 17% the maximum deviation occurred for the convection heat transfer coefficient at the off-gas side of the tubes α_{gas}. The minimum deviation occurred for the convection heat transfer coefficient at the oil side of the tubes α_{oil} being around 8.5%. Since the convection heat transfer coefficient for thermal oil is of one order greater than the coefficient for off-gas, the overall heat transfer coefficient U_o is dominated by the later one. Therefore the deviation of U_o (15.6%) is similar to the deviation of α_{gas}. Also the deviation of the heat flux $\dot{q}$ (17.1%) is almost the same like the deviation of α_{gas} indicating a consistency of the numerical results.

These deviations can be explained by the modeling of the wall roughness. The surfaces were modeled as smooth walls, but in practice the dust covering the tubes results in roughness and thereby increased turbulence around the tubes. A lower turbulence in the model results in decreased heat transfer coefficients. At the same time the lower turbulence in the model leads to a lower pressure drop for the off-gas than analytically determined (deviation: 10.9%).

By a sensitivity analysis, the turbulence intensity specified at the inlet of the model was found to have no influence on the numerical results. This indicates that the simulated turbulence around the eighth tube is caused by the upstream lying tubes and that the number of modeled tubes was chosen appropriately.

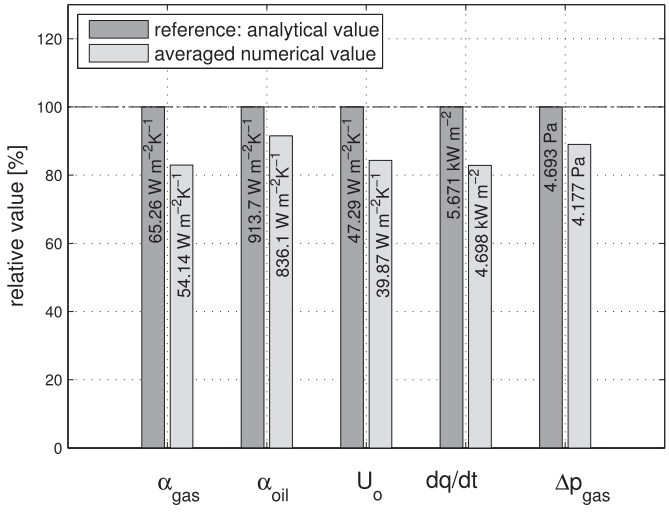

Fig. 11. Comparison between analytical and numerical results with indicated absolute values: pressure drop related to one row.

4. Conclusion

This paper shows the development and validation of a heat exchanger used to extract the waste heat from the off-gas from an EAF at a steel plant. The main constraints of the heat transfer on off-gas side are the high variation in off-gas temperature and velocity due to the discontinuous operation modus in combination with the high particle load. The waste heat is transferred to a thermal oil circuit by a tube bundle heat exchanger.

Experiments with single bare tubes and tube bundles within the off-gas channel system showed that fouling predominantly depends on the tube diameter as well as on the tube arrangement. Hence fouling can be significantly reduced by an appropriate tube bundle configuration and thus the cleaning effort can be minimized.

Based on these results as well as on comprising EAF off-gas and dust measurements an optimized heat exchanger configuration was determined using sensitivity analyses. Thereby the influence of the cross sectional area of the tube bundle and the diagonal pitch-to-diameter ratio on the overall heat transfer coefficient and the pressure drop was examined.

The analytically determined values of the reference heat exchanger configuration were compared to numerical results of CFD simulations. Pre-studies were conducted to identify both a suitable mesh and an acceptable grid resolution considering computational costs and numerical error. The optimized grid was applied to a model of a section of the heat exchanger. Using this model, representative results for the complete heat exchanger were calculated and compared to the analytical results. Deviations in the range of 8% for the convection heat transfer coefficient at the inner side of the tubes to 17% for the convection heat transfer coefficient at the outer side of the tubes were revealed. A reason therefore is the modeling of the tube surfaces as smooth walls. An increased turbulence due to the surface of the fouled tubes leads to an increased heat transfer and pressure loss.

Acknowledgements

The presented results are part of the federal joint research project “improvement of energy efficiency by electrifying waste heat from energy-intensive industrial processes” which was funded by the German DLR (2009–2011, FKZ 01LY0909B).

Nomenclature

A_{cs}	cross sectional area
A_{hx}	heat exchanger area
a	crosswise pitch-to-diameter ratio
b	streamwise pitch-to-diameter ratio
c	diagonal pitch-to-diameter ratio

D	inner off-gas channel diameter
d_i	inner tube diameter
d_o	outer tube diameter
f_A	arrangement factor
$f_{A,l,\mathrm{stag}}$	laminar component of the arrangement factor for staggered arrangement
$f_{A,\mathrm{stag}}$	arrangement factor for a staggered tube bundle
$f_{A,t,\mathrm{stag}}$	turbulent component of the arrangement factor for staggered arrangement
$f_{n,t}$	turbulent component of correction factor for number of rows
$f_{z,l}$	laminar component of correction factor for temperature dependence
$f_{z,t}$	turbulent component of correction factor for temperature dependence
$f_{zn,l}$	laminar component of correction factor for temperature dependence and number of rows
L	characteristic length
L_{bundle}	length of entire bundle
$\dot{m}_{\mathrm{gas}}$	mass flow off-gas
$\dot{m}_{\mathrm{oil}}$	mass flow thermal oil
n_o	number of obstacles
n_{oil}	passings of thermal oil
n_{rows}	number of rows
$n_{t/r}$	number of tubes per row
n_{tubes}	total number of tubes
Nu_{bundle}	Nusselt number of entire tube bundle
Nu_l	laminar component of Nusselt number a single row
Nu_{row}	Nusselt number of a single row
Nu_t	turbulent component of Nusselt number a single row
$p_{\mathrm{dyn,gas}}$	dynamic pressure off-gas
p_{dyn}	dynamic pressure
p_{in}	pressure at inlet
p_{out}	pressure at outlet
$p_{\mathrm{out,oil}}$	outlet pressure thermal oil
$p_{\mathrm{out,oil},t}$	outlet pressure of all tubes
$p_{\mathrm{ref,oil}}$	reference pressure of all thermal oil domains
$p_{\mathrm{rel,gas}}$	relative pressure at outlet of off-gas
$p_{\mathrm{stat,gas}}$	absolute static pressure off-gas
p_{stat}	static pressure
Pr	Prandtl number
$\dot{q}$	heat flux
$\dot{q}_{\mathrm{able}}$	transferable heat flux
$\dot{q}_{\mathrm{int}}$	intended heat flux
R_f	fouling factor
Re	Reynolds number
Re_ψ	Reynolds number for heat transfer
$\overline{Re}_{\mathrm{oil}}$	average Reynolds number thermal oil
s_d	dust layer thickness
T_w	wall temperature
T_{gas}	temperature off-gas
T_{in}	temperature at inlet
$T_{\mathrm{in,gas,1}}$	inlet temperature first tube thermal oil
$T_{\mathrm{in,gas}}$	inlet temperature off-gas
T_{out}	temperature at outlet
$T_{\mathrm{out,gas}}$	outlet temperature off-gas
$T_{\mathrm{out,oil}}$	outlet temperature thermal oil
U_o	overall heat transfer coefficient in relation to outer tube surface
W_{bundle}	width of entire bundle
w_f	average fluid velocity in free cross section of channel
w_n	average velocity in narrowest bundle section
w_{gas}	velocity off-gas
$w_{\mathrm{in,gas}}$	inlet velocity off-gas
$w_{\mathrm{in,oil}}$	inlet velocity thermal oil
y^+	dimensionless wall distance
α_{gas}	heat transfer coefficient on off-gas side of tubes (outer side)
α_{oil}	heat transfer coefficient on thermal oil side of tubes (inner side)
Δp_a	pressure drop due to acceleration
Δp_f	pressure drop due to friction
Δp_{gas}	pressure drop of off-gas
Δp_{tot}	total pressure drop
η	dynamic viscosity
η_W	dynamic viscosity at average wall temperature
λ	heat conductivity
λ_{steel}	heat conductivity of steel (1.4571)
ν	kinematic viscosity
ψ	void fraction
ρ	fluid density
ρ_{gas}	density off-gas
ξ	friction factor
ξ_l	laminar component of friction factor
ξ_t	turbulent component of friction factor

References

[1] U.S. Energy Information Administration, International Energy Outlook 2011, dOE/EIA-0484, September 2011.

[2] International Energy Agency, Paris, Worldwide Trends in Energy Use and Efficiency, 2008.

[3] World Steel Association, Brussels, Steel and Energy – Fact Sheet, 2008. URL, http://www.worldsteel.org/dms/internetDocumentList/fact-sheets/Fact-sheet_Energy/document/Fact%20sheet_Energy.pdf.

[4] D. Lindenberger, M. Bartels, F. Borggrefe, D. Bothe, R. Wissen, B. Hillebrand, et al., Studie Energiewirtschaftliches Gesamtkonzept 2030, VWEW Energieverlag GmbH, Frankfurt am Main, 2008, p. 213.

[5] M. Kirschen, Energieeffizienz und Emissionen der Lichtbogenöfen in der Stahlindustrie, first ed., Verlag Stahleisen GmbH, Düsseldorf, 2007, p. 15.

[8] L. Voj, Stickoxidemissionen von Lichtbogenöfen der Stahlindustrie (Dissertation), Fakultät für Georessourcen und Materialtechnik der RWTH Aachen, Aachen, 2006.

[9] M.Y. Kochnov, et al., Air pollution by large steel-melting arc furnaces, Steel Transl. 40 (5) (2010) 418–426.

[10] S. Gara, S. Schrimpfl, I. Schindler, Behandlung von Reststoffen und Abfällen in der Eisen- u. Stahlindustrie, Tech. Rep., Umweltbundesamt Austria, Wien (, 1997

[11] Deutsches Patent-und Markenamt, Verfahren zur Hydrometallurgischen Behandlung von Stahlwerk-Lichtbogen-Elektroofen(EAF)-Staub und die bei diesem Verfahren erhaltenen Pigmente, Veröffentlichung der internationalen Anmeldung mit der Veröffentlichungs-Nr. WO 2005/059038, Dt. Aktz.: DE 11 2004 002 509 T5, 29.03.2007 (2007).

[12] E.U. Kommission, Korrosion in Anlagen zur thermischen Abfallbehandlung; Entwicklung und Betrieb einer online Korrosionssonde Vorhaben EU 19-Sonde – Schlussbericht, 2007.

[13] D. Bouris, G. Papadakis, G. Bergeles, Numerical evaluation of alternate tube configurations for particle deposition rate reduction in heat exchanger tube bundles, Int. J. Heat. Fluid Flow 21 (2001) 525–536.

[15] V. Gesellschaft (Ed.), VDI Heat Atlas, second ed., Springer-Verlag, Berlin/Heidelberg/New York, 2010.

[16] S.B. Beale, D.B. Spalding, A numerical study of unsteady fluid flow in in-line and staggered tube banks, J. Fluids Struct. 13 (1999) 723–754.

[17] P. Rollet-Miet, D. Laurence, J. Ferziger, Les and rans of turbulent flow in tube bundles, Int. J. Heat Fluid Flow 20 (1999) 241–254.

[18] W. Polifke, J. Kopitz, Wärmeübertragung, second ed., Pearson Studium, München, 2009.

[19] H. Hausen, Wärmeübertragung im Gegenstrom, Gleichstrom und Kreuzstrom, second ed., Springer-Verlag, Berlin/Heidelberg/New York, 1976.

[20] E.-U. Schlünder, Heat Exchanger Design Handbook, first ed., Hemisphere Publishing Corporation, Washington, 1984.

[21] A. Žukauskas, Heat transfer from tubes in crossflow, Adv. Heat Transfer 8 (1987) 87–159.

[22] W. Khan, J. Culham, M. Yovanovich, Convection heat transfer from tube banks in crossflow: analytical approach, Int. J. Heat Mass Transfer 49 (2006) 4831–4838.

[23] J.H. Ferziger, M. Peri&cacute, Computational Methods for Fluid Dynamics, third ed., Springer-Verlag, Berlin/Heidelberg/New York, 2002.

[24] S. Benhamadouche, D. Laurence, Les, coarse les and transient rans comparisons on the flow across a tube bundle, Int. J. Heat Fluid Flow 24 (2003) 470–479.

[25] D. Bouris, G. Bergeles, Two dimensional time dependent simulation of the subcritical flow in a staggered tube bundle using a subgrid scale model, Int. J. Heat Fluid Flow 20 (1999) 105–114.

[26] S. Paul, et al., Experimental and numerical investigation of turbulent cross-flow in a staggered tube bundle, Int. J. Heat Fluid Flow 29 (2008) 387–414.
[27] P. Rodgers, A. Goharzadeh, O. Ali, V. Eveloy, An experimental and numerical investigation of tube bank heat exchanger thermofluids, in: Vorlesungsskript, 9th. Int. Conf. on Thermal, Mechanical and Multiphysics Simulation and Experiments in Micro-Electronics and Micro-Systems, EuroSimE, 2008.
[28] C. Brandt, J. Kuckelkorn, Steigerung der Energieeffizienz durch Verstromung von Abwärme aus energieintensiven Industrieprozessen – ORCmetall, Abschlussbericht zum Forschungsvorhaben FKZ 01LY0909B, ZAE Bayern, Garching, 2012.